

A general(ized) local rheology for wet granular materials

This content has been downloaded from IOPscience. Please scroll down to see the full text.

View [the table of contents for this issue](#), or go to the [journal homepage](#) for more

Download details:

IP Address: 130.89.77.245

This content was downloaded on 24/04/2017 at 12:13

Please note that [terms and conditions apply](#).

You may also be interested in:

[The role of gravity or pressure and contact stiffness in granular rheology](#)

Abhinendra Singh, Vanessa Magnanimo, Kuniyasu Saitoh et al.

[Granular and particle-laden flows: from laboratory experiments to field observations](#)

R Delannay, A Valance, A Mangeney et al.

[Shear thickening in concentrated suspensions: phenomenology, mechanisms and relations to jamming](#)

Eric Brown and Heinrich M Jaeger

[Anisotropy in cohesive, frictional granular media](#)

Stefan Luding

[2D and 3D confined granular chute flows: experimental and numerical results](#)

Weitao Bi, Renaud Delannay, Patrick Richard et al.

[Microrheology to probe non-local effects in dense granular flows](#)

Mehdi Bouzid, Martin Trulsson, Philippe Claudin et al.

[Force networks and the dynamic approach to jamming in granular media](#)

G. Lois and J. M. Carlson

[A positron emission particle tracking investigation of the flow regimes in tumbling mills](#)

I Govender and T Pathmathas

[Flow of dense granular material: towards simple constitutive laws](#)

O Pouliquen, C Cassar, P Jop et al.



PAPER

A general(ized) local rheology for wet granular materials

OPEN ACCESS

RECEIVED
12 September 2016REVISED
13 February 2017ACCEPTED FOR PUBLICATION
17 February 2017PUBLISHED
10 April 2017

Original content from this work may be used under the terms of the [Creative Commons Attribution 3.0 licence](https://creativecommons.org/licenses/by/4.0/).

Any further distribution of this work must maintain attribution to the author(s) and the title of the work, journal citation and DOI.



Sudeshna Roy, Stefan Luding and Thomas Weinhart

Multi-Scale Mechanics (MSM), MESA+, Engineering Technology, University of Twente, PO Box 217, 7500 AE Enschede, The Netherlands

E-mail: s.roy@utwente.nl

Keywords: granular materials, rheology, timescales, cohesion, shear thinning

Abstract

We study the rheology of dry and wet granular materials in the steady quasistatic regime using the discrete element method in a split-bottom ring shear cell with focus on the macroscopic friction. The aim of our study is to understand the local rheology of bulk flow at various positions in the shear band, where the system is in critical state. We develop a general(ized) rheology, in which the macroscopic friction is factorized into a product of four functions, on top of the classical $\mu(I)$ rheology, each of which depends on exactly one dimensionless control parameter, quantifying the relative importance of different micro-mechanical mechanisms. These four control parameters relate the time scales of shear rate $t_{\dot{\gamma}}$, particle stiffness t_k , gravity t_g and cohesion t_c , respectively, with the governing time scale of confining pressure t_p . While $t_{\dot{\gamma}}$ is large and thus of little importance for most of the slow flow data studied, it increases the friction in critical state, where the shear rate is high and decreases friction by relaxation (creep) where the shear rate is low. t_g and t_k are comparable to t_p in the bulk, but become more or less dominant relative to t_p at the extremes of low pressure at the free surface and high pressure deep inside the bulk, respectively. The effect of wet cohesion on the flow rheology is quantified by t_c decreasing with increasing cohesion. Furthermore, the proposed rheological model predicts well the shear thinning behavior both in the bulk and near the free surface; shear thinning rate becomes less near the free surface with increasing cohesion.

1. Introduction

The ability to predict a material's flow behavior, its rheology (like the viscosity for fluids) gives manufacturers an important product quantity. Knowledge on material's rheological characteristics is important in predicting the pourability, density and ease with which it may be handled, processed or used. The interrelation between rheology and other product dimensions often makes the measurement of viscosity the most sensitive or convenient way of detecting changes in flow properties. A frequent reason for the measurement of rheological properties can be found in the area of quality control, where raw materials must be consistent from batch to batch. For this purpose, flow behavior is an indirect measure of product consistency and quality.

Most studies on cohesive materials in granular physics focus on dry granular materials or powders and their flow [15, 39]. However, wet granular materials are ubiquitous in geology and many real-world applications where interstitial liquid is present between the grains. Many studies have applied the $\mu(I)$ -rheology to flows of dry materials at varying inertial numbers I [40, 41, 43, 45, 49]. Studies of wet granular rheology include flow of dense non-Brownian suspensions [3, 13, 14, 21]. Here, we study partially wetted system of granular materials, in particular the pendular regime, which is also covered in many studies [35, 38, 51]. While ideally, unsaturated granular media under shear show redistribution of liquid content among the contacts [28, 36], we assume a simplistic approach of homogeneous liquid content for liquid bridges of all contacts. One of the important aspects of partially wetted granular shear flows is the dependence of shear stress on the cohesive forces for wet materials. Various experimental and numerical studies show that addition of liquid bridge forces leads to higher yield strength. The yield stress at critical state can be fitted as a linear function of the pressure with the friction coefficient of dry flow μ_o as the slope and a finite offset c , defined as the steady state cohesion in the limit of zero

confining pressure [35]. This finite offset c is constant in the high pressure limit. However, very little is known regarding the rheology for granular materials in the low pressure limit.

Depending on the surrounding conditions, granular flows phenomenon are affected by appropriate time scales namely, t_p : time required for particles to rearrange under certain pressure, t_γ : time scale related to strain rate $\dot{\gamma}$, t_k : related to the contact time between particles, t_g : elapsed time for a single particle to fall through half its diameter under the influence of gravity and t_c : time scale for the capillary forces driving the flow are primarily hindered by inertia based on particle density. While various time scales, as related to the ongoing mechanisms in the sheared bulk of the material, can interfere, they also can get decoupled, in the extremes of the local/ global condition, if one time scale gets way smaller in magnitude than the other. A detailed description of this time scales are given in section 3. While t_k , t_g and t_c are global, other time scales t_γ and t_p depends on local field variables strain rate $\dot{\gamma}$ and pressure p respectively. We restrict our studies to the quasi-static regime ($t_\gamma \gg t_p$) as the effect of cohesion decreases with increasing inertial number due to the fast decrease in coordination number [1]. Moreover, the quasistatic regime observed for non-cohesive particles also persist for cohesive particles, while the inertial regime of noncohesive particles bifurcates into two regimes: rate-independent cohesive regime at low shear rates and inertial regime at higher shear rates [11]. In the present work, we shed light on the rheology of non-cohesive dry as well as cohesive wet granular materials at the small pressure limit, by studying free surface flow. While the inertial number I [19], i.e. the ratio of confining pressure to strain-rate time scales, is used to describe the change in flow rheology from quasi-static to inertial conditions, we look at additional dimensionless numbers that influence the flow behavior. (i) The local compressibility p^* , which is the squared ratio of the softness and stress time scales (ii) the inverse relative pressure gradient p_g^* , which is the squared ratio of gravitational and stress time scales and (iii) the Bond number Bo [48] quantifying local cohesion as the squared ratio of stress to wetting time scales are these dimensionless numbers. We show a constitutive relation based on these dimensionless numbers in sections 4–6 of this paper. Additional relevant parameters are not discussed in this study, namely granular temperature or fluidity. All these dimensionless numbers can be related to different time scales or force scales relevant to the granular flow.

Granular materials display non-Newtonian flow behavior for shear stresses above the so called *yield stress* while they remain mostly elastic like solids below this yield stress. More specifically, granular materials flow like a shear thinning fluid under sufficient stress. When dealing with wet granular materials, it is therefore of fundamental interest to understand the effect of cohesion on the bulk flow and yield behavior. Recently, the majority of investigations of non-Newtonian flow behavior focused on concentrated colloidal suspensions. Shear thickening is often observed in those flows due to the formation of flow-induced density fluctuations (hydroclusters) resulting from hydrodynamic lubrication forces between particles [46]. Similar local clusters (aggregates) can also be found in strongly cohesive wet granular materials, especially near to the free surface, where attractive forces dominate their repulsive counterparts [39]. However, the strong correlations observed between particles of close proximity in suspensions seem to be irrelevant in wet granular systems, where the range of force interactions is much more limited. On the other hand, Lin *et al* [22] show that contact forces dominate over hydrodynamic forces in suspensions that show continuous shear thickening. Fall *et al* [7] propose that discontinuous shear thickening of cornstarch suspensions is a consequence of dilatancy: the system under flow attempts to dilate but instead undergoes a jamming transition because it is confined—a phenomenon that was recently also explained by a moving jamming point [20]. Another possible cause for shear thickening is the large stress required to maintain flow due to particle–particle friction above a critical stress as in [6, 29]. This is more likely to happen in charge stabilized colloidal suspensions. Here we only intended to speculate the flow behavior of cohesive granular materials in relevance to micro scale analogy for shear thickening in suspensions and section 7 of this paper is devoted to understand more on the behavior of wet granular materials with increasing cohesion.

2. Model system

2.1. Geometry

2.1.1. Split-bottom ring shear cell

We use MercuryDPM [42, 50], an open-source implementation of the discrete particle method, to simulate a shear cell with annular geometry and a split bottom plate, as shown in figure 1. Some of the earlier studies in similar rotating set-ups include [37, 47, 52]. The geometry of the system consists of an outer cylinder (outer radius $R_o = 110$ mm) rotating around a fixed inner cylinder (inner radius $R_i = 14.7$ mm) with a rotation frequency of $\Omega = 0.01$ revolutions per second. The granular material is confined by gravity between the two concentric cylinders, the bottom plate, and a free top surface. The bottom plate is split at radius $R_s = 85$ mm. Due to the split at the bottom, a narrow shear band is formed. It moves inwards and widens towards the flow surface. This set-up thus features a wide shear band away from the bottom and the side walls which is thus free

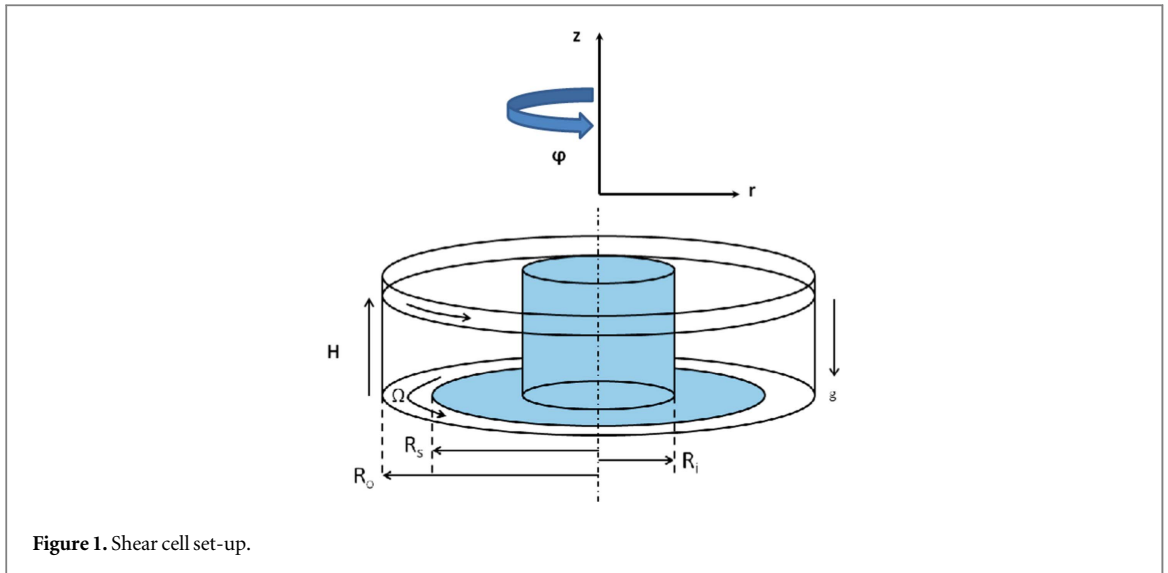


Figure 1. Shear cell set-up.

Table 1. Table showing the particle properties and constant contact model parameters.

Parameter	Symbol	Value
Sliding friction coefficient	μ_p	0.01
Normal contact stiffness	k	120 N m^{-1}
Viscous damping coefficient	γ_o	$0.002 \text{ kg}^{-1} \text{ s}$
Rotation frequency	Ω	0.01 s^{-1}
Particle density	ρ	2000 kg m^{-3}
Gravity	g	9.81 m s^{-2}
Mean particle diameter	d_p	2.2 mm
Contact angle	θ	20°
Liquid bridge volume	V_b	75 nl

from boundary effects. The filling height ($H = 40 \text{ mm}$) is chosen such that the shear band does not reach the inner wall at the free surface.

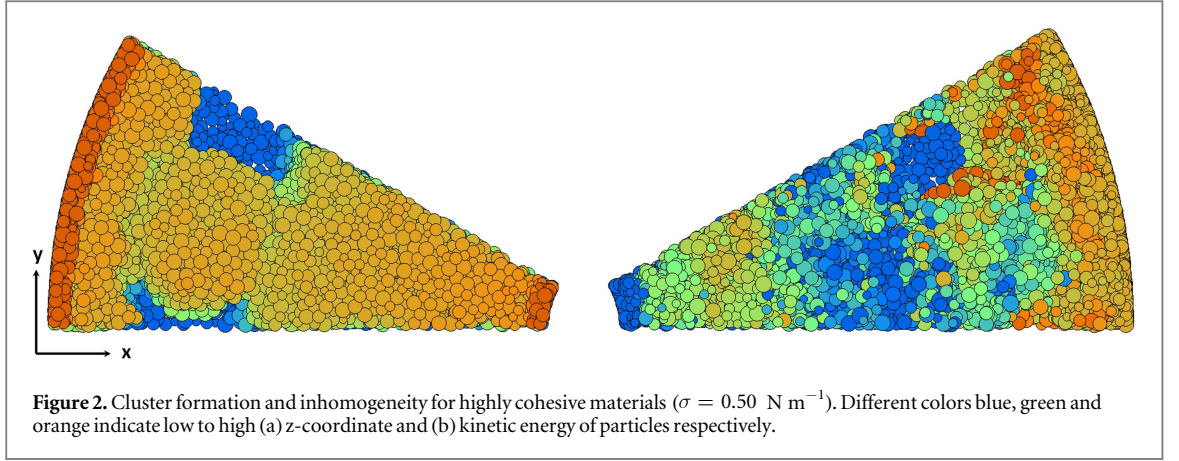
In earlier studies [33, 39, 40], a quarter of this system ($0^\circ \leq \phi \leq 90^\circ$) was simulated using periodic boundary conditions. In order to save computation time, here we simulate only a smaller section of the system ($0^\circ \leq \phi \leq 30^\circ$) with appropriate periodic boundary conditions in the angular coordinate, unless specified otherwise. We have observed no noticeable effect on the macroscopic behavior in comparisons between simulations done with a smaller (30°) and a larger (90°) opening angle. Note that for very strong attractive forces, agglomeration of particles occur. Then, a higher length scale of the geometry is needed and thus the above statement is not true anymore.

2.2. Contact model and parameters

The liquid bridge contact model is based on a combination of an elastic-dissipative linear contact model for the normal repulsive force and a nonlinear irreversible liquid bridge model for the non-contact adhesive force as described in [35]. The adhesive force is determined by three parameters; surface tension σ , contact angle θ which determine the maximum adhesive force and the liquid bridge volume V_b which determines the maximum interaction distance between the particles at the point of bridge rupture. The contact model parameters and particle properties are as given in table 1. We have a polydisperse system of glass bead particles with mean diameter $d_p = \langle d \rangle = 2.2 \text{ mm}$ and a gaussian size distribution ($d_{\min}/d_{\max} = 1/2$ of width $1 - \langle d \rangle^2 / \langle d^2 \rangle \approx 0.04$).

To study the effect of inertia and contact stiffness on the non-cohesive materials rheology, we compare our data for non-cohesive case with data from simulations of [40] for different gravity as given below:

$$g \in \{1.0, 2.0, 5.0, 10.0, 20.0, 50.0\} \text{ m s}^{-2}. \quad (1)$$



We also compare the effect of different rotation rates on the rheology for the following rotation rates:

$$\Omega \in \{0.01, 0.02, 0.04, 0.10, 0.20, 0.50, 0.75, 1.00\} \text{ rps.} \quad (2)$$

The liquid capillary force is estimated as stated in [51]. It is observed in our earlier studies [35] that the shear stress τ for high pressure can be described by a linear function of confining pressure, p , as $\tau = \mu_o p + c$. It was shown that the steady state cohesion c is a linear function of the surface tension of the liquid σ while its dependence on the volume of liquid bridges is defined by a cube root function. The friction coefficient μ_o is constant and matches the friction coefficient of dry flows excluding the small pressure limit. In order to see the effect of varying cohesive strength on the macroscopic rheology of wet materials, we vary the intensity of capillary force by varying the surface tension of the liquid σ , with a constant volume of liquid bridges ($V_b = 75 \text{ nl}$) corresponding to a saturation of 8%, as follows:

$$\sigma \in \{0.0, 0.01, 0.02, 0.04, 0.06, 0.10, 0.20, 0.30, 0.40, 0.50\} \text{ N m}^{-1}. \quad (3)$$

The first case, $\sigma = 0.0 \text{ N m}^{-1}$, represents the case of dry materials without cohesion, whereas $\sigma = 0.50 \text{ N m}^{-1}$ corresponds to the surface tension of a mercury–air interface. For $\sigma > 0.50 \text{ N m}^{-1}$, smooth, axisymmetric shear band formation is not observed and the materials agglomerate to form clusters as shown in figure 2, for our particle size and density. Hence, σ is limited to maximum of 0.50 N m^{-1} .

2.3. Averaging methodology

To extract the macroscopic properties, we use the spatial coarse-graining approach detailed in [24–26]. The averaging is performed over a grid of 47-by-47 toroidal volumes, over many snapshots of time assuming rotational invariance in the tangential ϕ -direction. The averaging procedure for a three-dimensional system is explained in [24, 26]. This spatial coarse-graining method was used earlier in [26, 33, 39, 40, 52]. We do the temporal averaging of non-cohesive simulations over a larger time window from 30 to 440 s with 2764 snapshots to ensure the rheological models with enhanced quality data. All the other simulations are run for 200 s and temporal averaging is done when the flow is in steady state, between 80 and 200 s with 747 snapshots, thereby disregarding the transient behavior at the onset of the shear. In the critical state, the shear band is identified by the region having strain rates higher than 80% of the maximum strain rate at the corresponding height. Most of the analysis explained in the later sections are done from this critical state data at the center of the shear band.

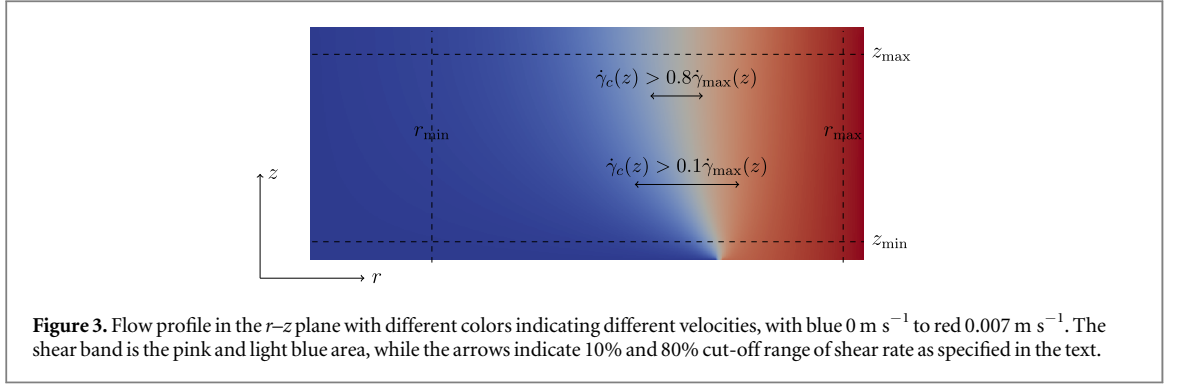
2.3.1. Macroscopic quantities

The general definitions of macroscopic quantities including stress and strain rate tensors are included in [40]. Here, we define the derived macroscopic quantities such as the friction coefficient and the apparent viscosity which are the major subjects of our study.

The local macroscopic friction coefficient is defined as the ratio of shear to normal stress and is defined as $\mu = \tau/p$.

The magnitude of strain rate tensor in cylindrical polar coordinates is simplified, assuming $u_r = 0$ and $u_z = 0$:

$$\dot{\gamma} = \frac{1}{2} \sqrt{\left(\frac{\partial u_\phi}{\partial r} - \frac{u_\phi}{r}\right)^2 + \left(\frac{\partial u_\phi}{\partial z}\right)^2}. \quad (4)$$



The apparent shear viscosity is given by the ratio of the shear stress and strain rate as:

$$\eta = \frac{\tau}{\dot{\gamma}} = \frac{\mu p}{\dot{\gamma}}, \quad (5)$$

where $\dot{\gamma}$ is the strain rate.

2.4. Critical state

We obtain the macroscopic quantities by temporal averaging as explained in section 2.3. Next we analyze the data, neglecting data near walls ($r < r_{\min} \approx 0.045 \text{ m}$, $r > r_{\max} \approx 0.105 \text{ m}$, $z < z_{\min} \approx 0.004 \text{ m}$) and free surface ($z > z_{\max} \approx 0.035 \text{ m}$) as shown in figure 3. Further, the consistency of the local averaged quantities also depends on whether the local data has achieved the critical state. The critical state is defined by the local shear accumulated over time under a constant pressure and constant shear rate condition. This state is reached after large enough shear, when the materials deform with applied strain without any change in the local quantities, independent of the initial condition. We focus our attention in the region where the system can be considered to be in the critical state and thus has a well defined macroscopic friction. To determine the region in which the flow is in critical state, $\dot{\gamma}_{\max}(z)$ is defined to be the maximum strain rate for a given pressure, or a given height z . The critical state is achieved at a constant pressure and strain rate condition over regions with strain rate larger than the strain rate $0.1\dot{\gamma}_{\max}(z)$ as shown in figure 3 corresponding to the region of shear band. While [40] showed that for rotation rate 0.01 rps, the shear band is well established above shear rate $\dot{\gamma} > 0.01 \text{ s}^{-1}$, of our analysis shown in the latter sections are in the shear band center is obtained by $\dot{\gamma} > 0.8\dot{\gamma}_{\max}(z)$ at different heights in the system. This is defined as the region where the local shear stress τ becomes independent of the local strain rate $\dot{\gamma}$ and τ/p becomes constant. We also extend our studies to the shear-rate dependence in critical state which is effective for critical state data for wider regions of shear band (section 4.4). This shear rate dependence is analyzed in the regions of strain rate ($\dot{\gamma}$) larger than the $0.1\dot{\gamma}_{\max}(z)$ at a given height z . These data include the region from the center to the tail of the shear band, with typical cut-off factors $s_c = 0.8$ or 0.1 , respectively, as shown in figure 3, and explained in section 4.4.

3. Time scales

Dimensional analysis is often used to define the characteristic time scales for different physical phenomena that the system involves. Even in a homogeneously deforming granular system, the deformation of individual grains is not homogeneous. Due to geometrical and local parametric constraints at grain scale, grains are not able to displace as affine continuum mechanics dictates they should. The flow or displacement of granular materials on the grain scale depends on the timescales for the local phenomena and interactions. Each time scale can be obtained by scaling the associated parameter with a combination of particle diameter d_p and material density ρ . While some of the time scales are globally invariant, others are varying locally. The dynamics of the granular flow can be characterized based on different time scales depending on local and global variables. First, we define the time scale related to contact duration of particles which depends on the contact stiffness k as given by [40]:

$$t_k = \sqrt{\frac{\rho d_p^3}{k}}. \quad (6)$$

In the special case of a linear contact model, this is invariant and thus represents a global time scale too. Two other time scales are globally invariant, the cohesive time scale t_c , i.e. the time required for a single particle to traverse a length scale of $d_p/2$ under the action of an attractive capillary force and the gravitational time scale t_g , i.e. the elapsed time for a single particle to fall through half its diameter d_p under the influence of the gravitational force. The time scale t_c could vary locally depending on the local capillary force f_c . However, the capillary force is

weakly affected by the liquid bridge volume while it strongly depends on the surface tension of the liquid σ . This leads to the cohesion time scale as a global parameter given by:

$$t_c = \sqrt{\frac{\rho d_p^4}{f_c}} \propto \sqrt{\frac{\rho d_p^3}{\sigma}}, \quad (7)$$

with surface tension σ and capillary force $f_c \approx \pi \sigma d_p$. The corresponding time scale due to gravity which is of significance under small confining stress close to the free surface is defined as:

$$t_g = \sqrt{\frac{d_p}{g}}. \quad (8)$$

The global time scales for granular flow are complemented by locally varying time scales. Granular materials subjected to strain undergo constant rearrangement and thus the contact network re-arranges (by extension and compression and by rotation) with a shear rate time scale related to the local strain rate field:

$$t_\gamma = \frac{1}{\dot{\gamma}}. \quad (9)$$

Finally, the time for rearrangement of the particles under a certain pressure constraint is driven by the local pressure p . This microscopic local time scale based on pressure is:

$$t_p = d_p \sqrt{\frac{\rho}{p}}. \quad (10)$$

As the shear cell has an unconfined top surface, where the pressure vanishes, this time scale varies locally from very low (at the base) to very high (at the surface). Likewise, the strain rate is high in the shear band and low outside, so that also this time scale varies between low and high, respectively.

Dimensionless numbers in fluid and granular mechanics are a set of dimensionless quantities that have a dominant role in describing the flow behavior. These dimensionless numbers are often defined as the ratio of different time scales or forces, thus signifying the relative dominance of one phenomenon over another. In general, we expect five time scales (t_g , t_p , t_c , t_γ and t_k) to influence the rheology of our system. Note that among the five time scales discussed here, there are ten possible dimensionless ratios of different time scales. We propose four of them that are sufficient to define the rheology that describes our results. Interestingly, all these four dimensionless ratios are based on the common time scale t_p . Thus, the time scale related to confining pressure is important in every aspect of the granular flow. All the relevant dimensionless numbers in our system are discussed in brief in the following two sections of this paper for the sake of completeness, even though not all are of equal significance.

4. Rheology of dry granular materials

4.1. Effect of softness in the bulk of the materials

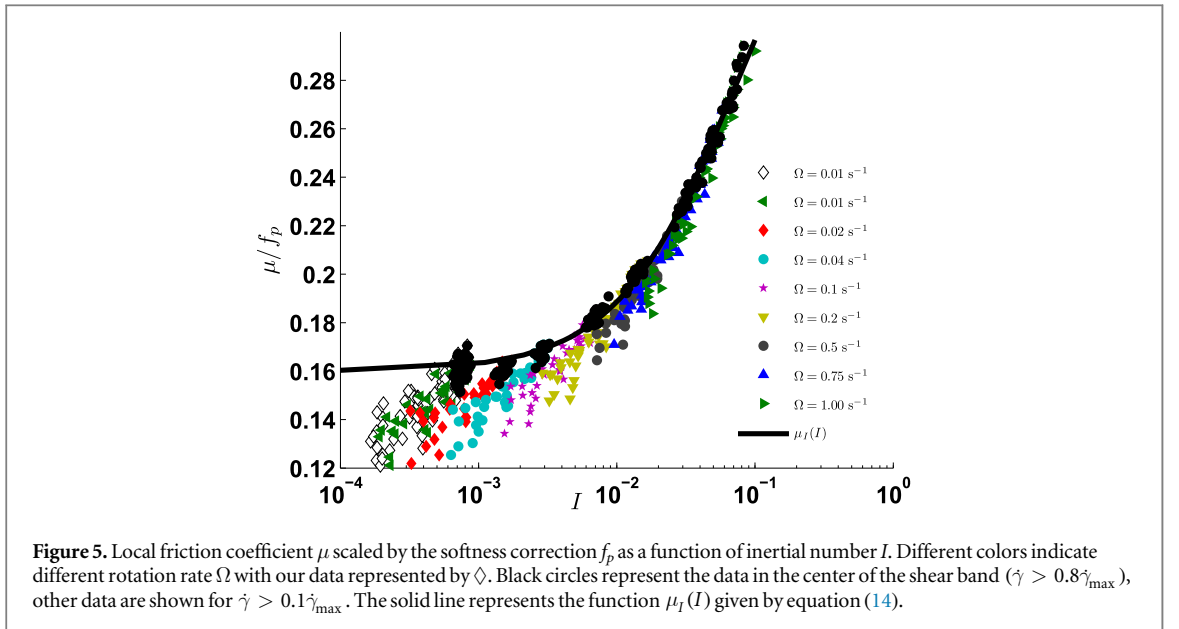
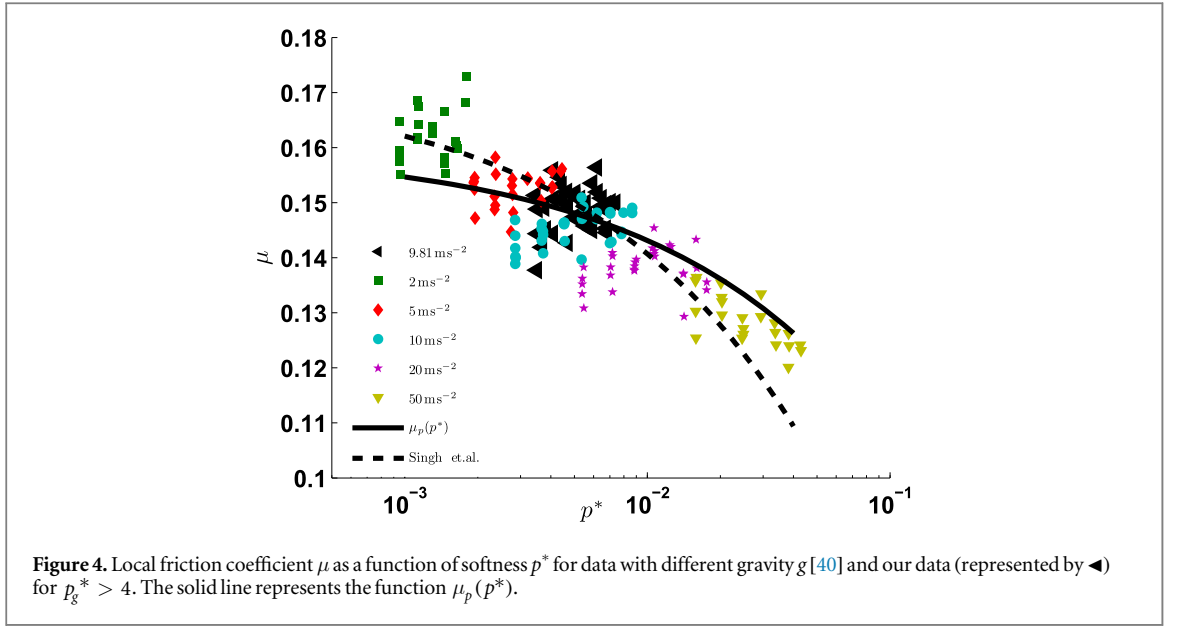
We study here the effect of softness on macroscopic friction coefficient for different gravity in the system. Thus the pressure proportional to gravity is scaled in dimensionless form p^* [40] given by:

$$p^* = \frac{p d_p}{k}. \quad (11)$$

This can be interpreted as the square of the ratio of time scales, $p^* = t_k^2/t_p^2$, related to contact duration and pressure respectively. Figure 4 shows the macroscopic friction coefficient as a function of the dimensionless pressure p^* and the dashed line is given by:

$$\mu_p(p^*) = \mu_o f_p(p^*) \quad \text{with} \quad f_p(p^*) = [1 - (p^*/p_o^*)^\beta], \quad (12)$$

where, $\beta \approx 0.50$, $\mu_o = 0.16$, $p_o^* \approx 0.90$. p_o^* denotes the limiting dimensionless pressure around the correction due to softness of the particles, where the correction is not applicable anymore, since $f_p \leq 0$ for $p^* \geq p_o^*$ [27]. We have used this fit, as our data range is too limited to derive the functional form of the fit. This is shown by the solid line in figure 4 with the plotted data from our present simulation (\blacktriangleleft) and with data for different gravity in the system [40] which we use to describe other corrections for dry non-cohesive materials. Despite the deviation of data for different gravity from the trend for small p^* , the agreement with our data is reasonable. The dashed line represents the softness correction as proposed by [40]. The effect of softness is dominant in regions of large pressure where the pressure time scale t_p dominates over the stiffness time scale t_k and thus the data in plot are corresponding to higher than a critical pressure ($p_g^* > 4$, explained in section 4.3). Here, the compressible forces dominate over the rolling and sliding forces on the particles, the flow being driven by squeeze. Thus, the macroscopic friction coefficient decreases with softness.



4.2. Effect of inertial number

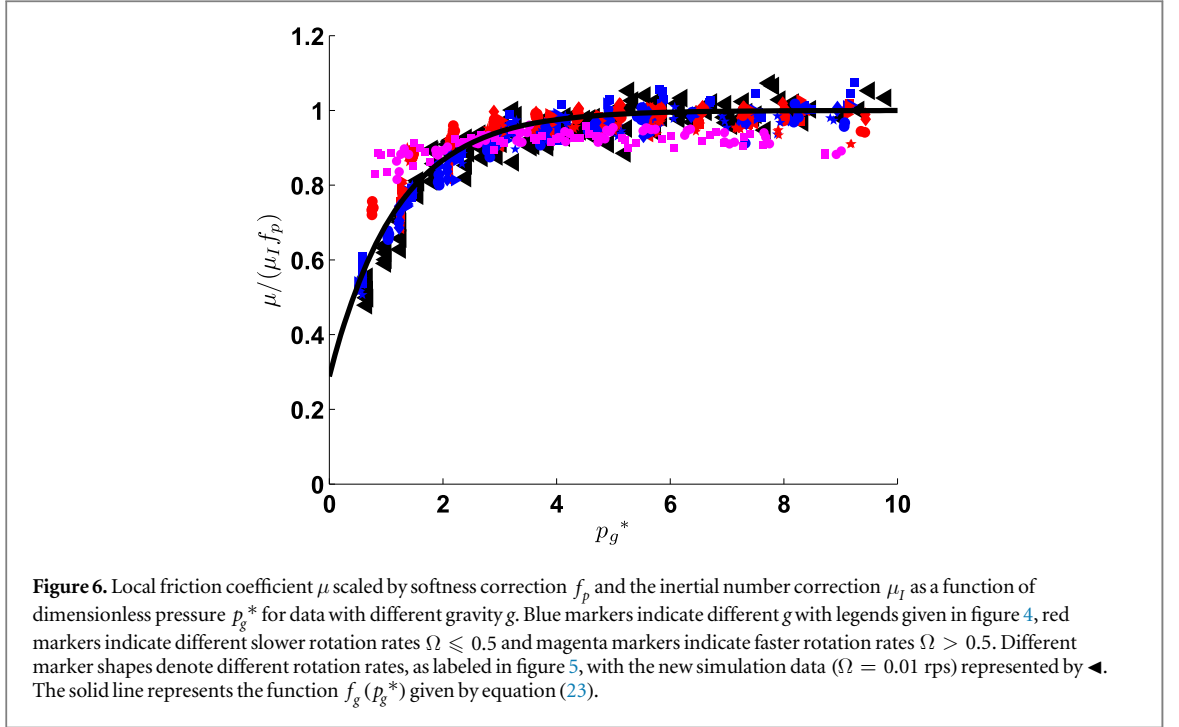
For granular flows, the rheology is commonly described by the dimensionless inertial number [30]:

$$I = \dot{\gamma} d_p / \sqrt{p/\rho}, \quad (13)$$

which can be interpreted as the ratio of the time scales, t_p for particles to rearrange under pressure p , and the shear rate time scale $t_\dot{\gamma}$ for deformation due to shear flow, see section 3. It has been shown both experimentally [10, 16, 30] and in simulations [31] that for intermediate inertial numbers (in the range $I \leq I_o$), the macroscopic friction coefficient follow the so-called $\mu(I)$ rheology:

$$\mu_I(I) = \mu_o + (\mu_\infty - \mu_o) \frac{1}{1 + I_o/I}. \quad (14)$$

We assume the combined effect of softness and inertial number given as $\mu(p^*, I) = \mu_I(I)f_p$ and thus analyze μ/f_p as a function of I , see figure 5. We compare our data for non-cohesive materials which is shown to be in agreement with the trend of data obtained from [40] for different external rotation rates. The black solid line corresponds to the data in the shear band center ($\dot{\gamma} > 0.8\dot{\gamma}_{\max}$) fitted by equation (14) with $\mu_o = 0.16$, $\mu_\infty = 0.40$ and $I_o = 0.07$ which are in close agreement with the fitting constants explained in [27]. Note that these fitting constants change with the range of I that are included in the fitting. Given that we do not have data



for very high inertial number from our simulations, our present fit shows $I_o \approx 0.07$ and hence the fit is valid for $I \leq I_o$.

4.3. Effect of gravity close to the free surface

In this section, we investigate the effect of the another dimensionless number p_g^* on local friction coefficient, given by:

$$p_g^* = \frac{p}{\rho d_p g}. \quad (15)$$

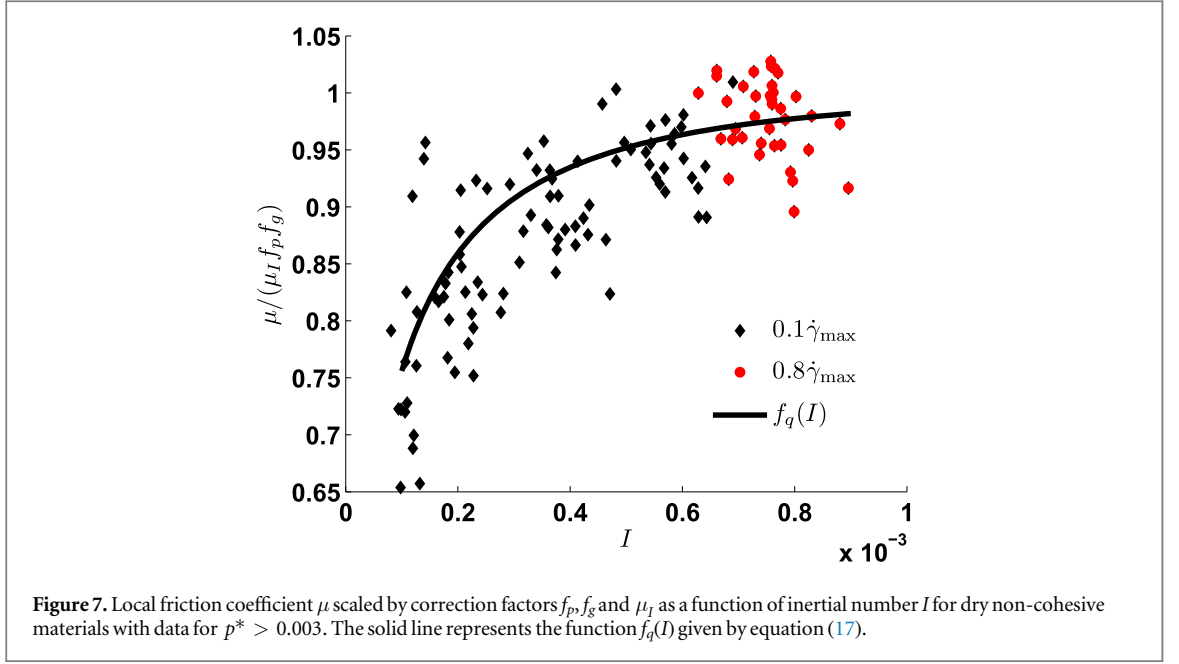
This can be interpreted as the square of the ratio of time scales, $p_g^* = t_g^2/t_p^2$, related to gravity and pressure respectively. The effect of inertial number and softness correction are eliminated by scaling μ by the correction factors μ_I and f_p respectively and studying the effect of p_g^* on the scaled friction coefficient. Figure 6 shows μ scaled by $\mu_I f_p$ as a function of dimensionless pressure p_g^* for different gravity g (different p^*) and different rotation rates Ω (different I), including our data for $g = 9.81 \text{ ms}^{-2}$ and $\Omega = 0.01$ rps which is also in agreement with other data set. The data for different slower rotation rates and different gravitational accelerations g agree well with our new data set, while the higher rotation rates deviate. Note that the higher rotation rates are in a different regime where kinetic theory works and hence agreement with the generalized rheology is not expected strictly. All the data for different gravity and slower rotation rates collapse and these can be fitted by the solid line given by the correction $f_g(p_g^*)$ where:

$$\mu_g(p_g^*) = \mu_o f_g(p_g^*) \quad \text{with} \quad f_g(p_g^*) = \left[1 - a' \exp\left(-\frac{p_g^*}{p_{go}^*}\right) \right], \quad (16)$$

where, $a' \approx 0.71$ is the relative drop in friction coefficient at $p_g^* = 0$, $p_{go}^* \approx 1.19$ is the dimensionless pressure at which the friction coefficient drops below $0.74\mu_o$ and $f_g(p_g^*)$ is the correction corresponding to the dimensionless pressure p_g^* . Due to lack of confining stress close to the free surface ($p_g^* < 4$), the macroscopic friction coefficient exponentially decreases with decrease in p_g^* . Here, the gravity time scale t_g dominates over the pressure time scale t_p . Thus, while the effect of gravity close to the free surface is dominant for $p_g^* < 4$, $p_g^* \approx 4$ is the critical pressure above which the effect of softness p^* is significant as explained in section 4.1.

4.4. Shear rate dependence in critical state flow

After having quantified the dependence of the macroscopic friction on inertial number and softness, another correction was proposed in [40], taking into account a reduced, relaxed friction correction in very slow quasi-static flow. The same phenomena was addressed in [17, 19, 24] using non-local constitutive relations. Figure 7



is a representation of this correction $f_q(I)$ where:

$$\mu_q(I) = \mu_o f_q(I) \quad \text{with} \quad f_q(I) = \left[1 - \exp\left(-\left(\frac{I}{I^*}\right)^{\alpha_1}\right) \right], \quad (17)$$

where, $I^* = (4.85 \pm 1.08) \times 10^{-5}$ for very small inertial numbers ($I \leq I^*$) and $\alpha_1 = 0.48 \pm 0.07$. This correction is in inspiration with [24] where I^* scales linearly with the external shear rate and thus is proportional to the local strain-rate and the granular temperature. Although the data represented in figure 7 (black \diamond and red \circ) include $\dot{\gamma}_c(z) > 0.1 \dot{\gamma}_{\max}(z)$, the fitted solid line given by $f_q(I)$ correction corresponds to data in the shear band center as well as outside center (for $\dot{\gamma}_c(z) > 0.1 \dot{\gamma}_{\max}(z)$) which are all in the critical state. Typically, we study the local effect for data inside the shear band center ($\dot{\gamma}_c(z) > 0.8 \dot{\gamma}_{\max}(z)$) which corresponds to the data given by red \circ which are invariant to the effect of small inertial number which allows us to assume $f_q(I) \approx 1.0$. Hence, in the following sections, we do not take into consideration the correction $f_q(I)$, though we mention it.

5. Rheology of wet-cohesive granular materials

5.1. Bond number

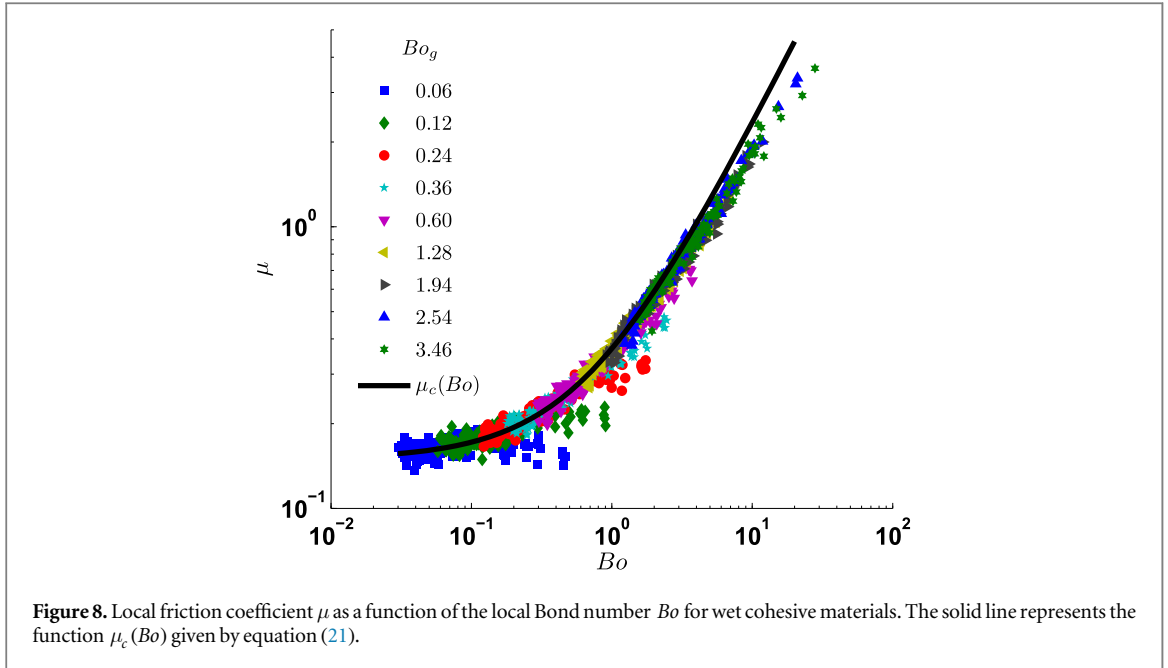
The Bond number (Bo) is a measure of the strength of the adhesive force relative to the compressive force. A low value of Bo (typically much less than 1) indicates that the system is relatively unaffected by the attractive forces; high Bo indicates that the attractive force dominates in the system. Thus Bo is a critical microscopic parameter that controls the macroscopic local rheology of the system. While the conventional way of defining the Bond number as the ratio of the time scales t_c and t_g [48] is appropriate for single particles, or close to the free surface, we define the local Bond number relative to the confining force:

$$Bo(p) = \frac{f_c^{\max}}{p d_p^2}, \quad (18)$$

defined as the square of the ratio between timescales related to pressure t_p and wetting time scale t_c . $f_c^{\max} = 2\pi r \gamma \cos \theta$ is the maximum capillary force between a pair of particles, where r is the effective radius of the interacting pair of particles. This provides an estimate of the local cohesion intensity by comparing the maximum capillary pressure allowed by the contact model f_c^{\max} / d_p^2 with the local pressure. A low to high transition of local Bond number from the bottom of the shear cell to the free surface is as a result of the change in time scale related to pressure t_p from $t_p \ll t_c$ to $t_p \gg t_c$ respectively. Subsequently, we define the global Bond number Bo_g as a measure of the strength of cohesion in the system as:

$$Bo_g = \frac{f_c^{\max}}{p^{\text{mean}} d_p^2}, \quad (19)$$

where, p^{mean} is the mean pressure in the system. This is an experimentally measurable quantity and is related to quantifying the system as a whole. The global Bond number corresponding to surface tension of liquid defined



in equation (3) is given by:

$$Bo_g \in \{0.0, 0.06, 0.12, 0.24, 0.36, 0.60, 1.28, 1.94, 2.54, 3.46\}. \quad (20)$$

5.1.1. Effect of local bond number

The properties of the particles and the interstitial fluid strongly affect the macroscopic behavior of granular materials. The local macroscopic friction is studied as a function of local Bond number Bo for different wet cohesion intensity. Figure 8 shows the macroscopic friction coefficient as a function of the local Bond number Bo for different wet cohesion. It is evident that the friction coefficient increases with local Bond number with a constant value μ_o in the low Bond number limit. For frictionless wet cohesive materials, the rheology can be defined by a linear fitting function given by:

$$\mu_c(Bo) = \mu_o f_c(Bo) \quad \text{with} \quad f_c(Bo) = (1 + aBo), \quad (21)$$

where, $\mu_o = 0.15$ is the macroscopic friction coefficient in the high pressure limit [35] and $a \approx 1.47$. This is shown by the solid line in figure 8. However, it is observed that the data deviate from the solid fitting line in the high Bond number or low pressure limit. This deviation is explained by the small pressure correction $f_g(p_g^*)$ as explained in section 4.3 and discussed in details in the next section.

5.2. Effect of gravity close to the free surface for wet materials

Figure 6 shows the dependence of the local friction coefficient on the local scaled pressure p_g^* for dry non-cohesive materials and this effect is small in the high pressure limit. With an attempt to separate the effect of Bond number on the rheology of cohesive materials, we plot the local friction coefficient μ scaled by the Bond number correction f_c and other corrections μ_I and f_p , as a function of scaled pressure p_g^* as shown in figure 9. The solid line is given by equation (23), where the non-cohesive function fits for the wet data as well.

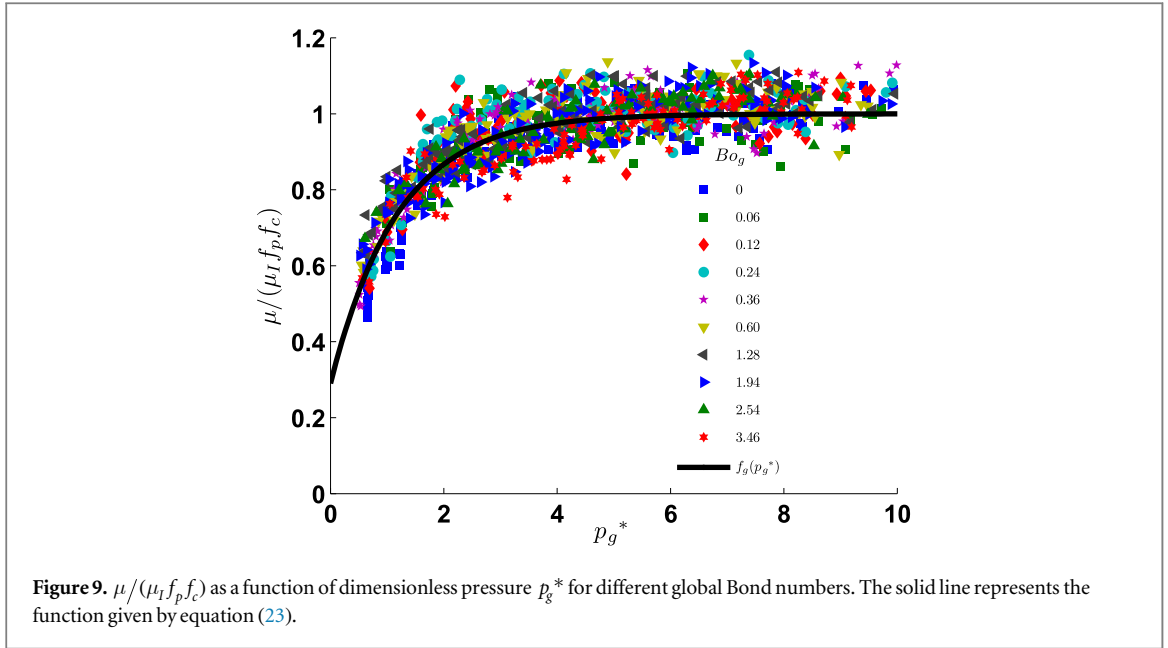
6. Rheological model

We studied the rheology of dry and wet granular materials in terms of different dimensionless numbers. The trends are combined and shown to collectively contribute to the rheology as multiplicative functions given by:

$$\mu(I, p^*, p_g^*, Bo) = \mu_I(I) f_g(p_g^*) f_q(I) f_c(Bo) f_p(p^*). \quad (22)$$

The proposed general(ized) multiplicative rheology function for the macroscopic friction coefficient is dependent on four dimensionless numbers p^* , p_g^* , I and Bo . Table A1 in the appendix gives the summary and details of our proposed rheological model.

This rheological model is based on constant liquid bridge volume at all contacts and we do not take into account liquid redistribution among contacts [28, 36]. This is a simplified approach to establish the generalized



rheology and we are working further on liquid redistribution and will analyze its effect on the rheology. However, the cohesion time scale is only weakly affected by the liquid bridge volume and mainly depends on the surface tension of the liquid. Preliminary results using a liquid redistribution model show that in this state, 40% of the contacts in the shear band center become dry, resulting in a higher probability of dry contacts with micro-contact local Bond number $Bo = 0$. This results in a lower local Bond number in the shear band center. Our present rheological model is shown to be valid for a wide range of Bond number and thus use of a liquid redistribution model is expected to shift data further, towards the lower Bond numbers but is expected to follow the same trends.

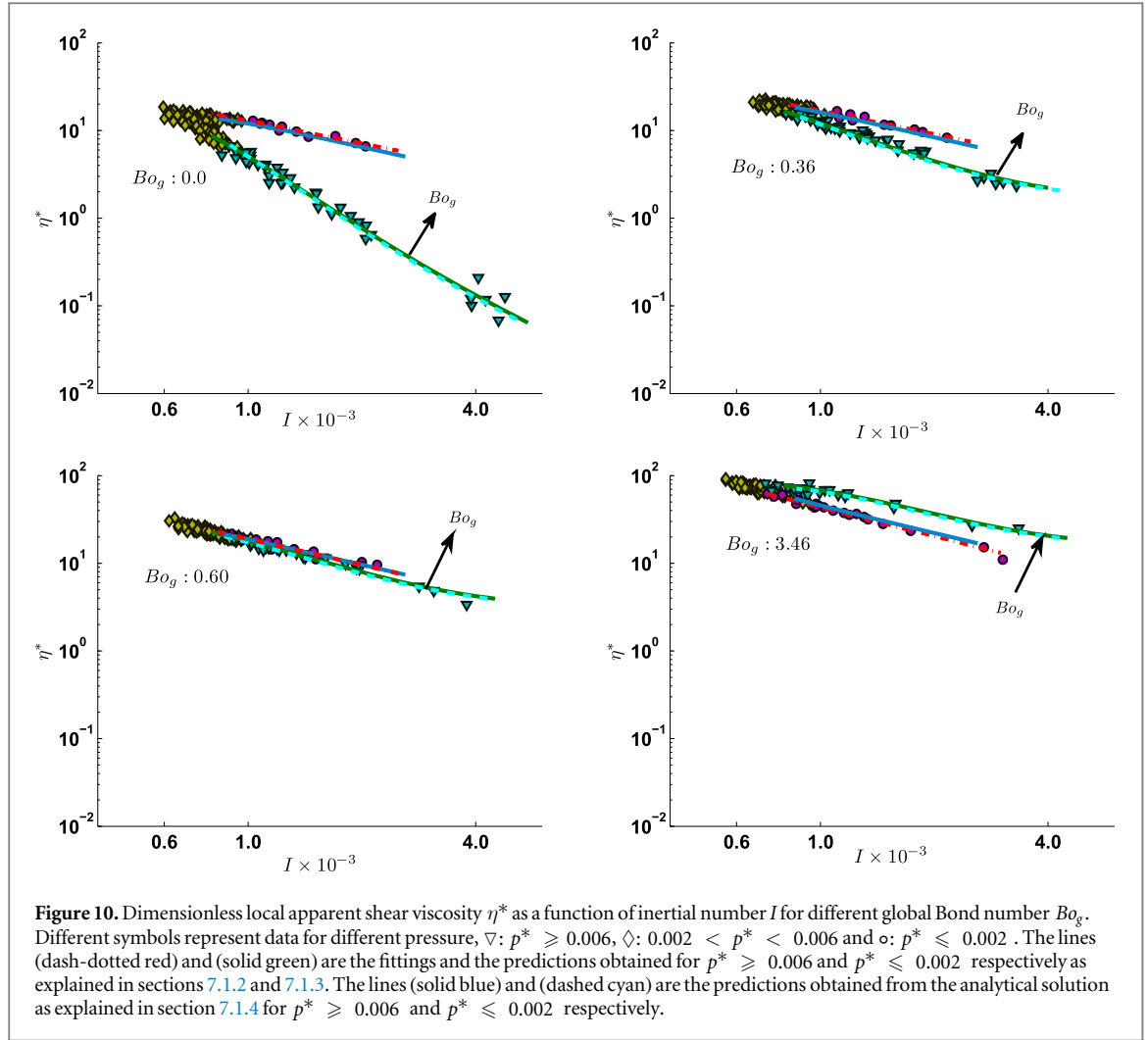
For a full constitutive law, one also needs to take into account the solid volume fraction also. For dry granular shear flow [27, 40], the constitutive relations for the volume fraction given by corrections (to first order) based on dimensionless numbers p^* and I as follows:

$$\phi(I, p^*) = \phi_c \left(1 + \frac{p^*}{p_c^*} \right) \left(1 - \frac{I}{I_c} \right), \quad (23)$$

where, $\phi_c \approx 0.65$ is the critical or the steady state density under shear, in the limit of vanishing pressure and inertial number. $I_c = 0.85$ is the inertial number corresponding to strain rate when the dilation turns to fluidization. $p_c^* = 0.33$ is the typical pressure for which softness leads to huge densities. Though the volume fraction in an inhomogeneous system is a field (fluctuating around a mean value), its local values are captured by the above equation in terms of the local dimensionless numbers. The above relation shows that the volume fraction decreases (and the friction increases) when the quasi-static regime is exceeded. However, the generalized rheology is expected to be valid everywhere in the inhomogeneous system where the system has been sheared long enough to reach the critical state, irrespective of their different volume fraction. The volume fraction increases with increase in confining stress as shown in [27, 40]. In ongoing research [34], we show that inter-particle cohesion has a considerable impact on the compaction of the soft materials. Cohesion causes additional stresses, due to capillary forces between particles, leading to an increase in volume fraction due to higher compaction. This effect is not visible in a system of infinitely stiff particles. On the other hand, we observe a general decrease in volume fraction due to increased cohesion, which we attribute to structural changes in the bulk material.

7. Local apparent viscosity

For unsaturated granular materials, being heterogeneous systems, it is not relevant to define their viscosity. Nevertheless, we introduce the local apparent viscosity η of granular materials which is barely the ratio of the shear stress to the strain rate as an alternative to μ . To see the combined effect of pressure and strain rate on the local apparent viscosity, we analyze them as functions of the inertial number. For a given pressure, the inertial number is proportional to the shear rate. Thus, the analysis of local apparent viscosity as a function of the inertial number for small pressure ranges can be interpreted as the analysis of apparent viscosity versus strain rate. We



define the dimensionless local apparent viscosity as:

$$\eta^* = \frac{\eta}{\sqrt{d_p k \rho}} = \frac{\mu p / \dot{\gamma}}{\sqrt{d_p k \rho}} = \frac{\mu \sqrt{p^*}}{I}. \quad (24)$$

Since we here focus on the data in the center of the shear band, the dependence on shear rate in the critical state flow which includes data outside the shear band center can be neglected ($f_q(I \geq I^*) \approx 1$) and thus the rheological model for the local friction coefficient given by equation (22) is simplified by:

$$\mu(p^*, p_g^*, Bo) = \mu_I(I) f_g(p_g^*) f_c(Bo) f_p(p^*). \quad (25)$$

The dimensionless variable η^* can be related to three time scales namely, contact duration t_k strain rate related time scale $t_{\dot{\gamma}}$ and pressure related time scale t_p as $\eta^* = \mu t_{\dot{\gamma}} t_k / t_p^2$.

Alternatively, the flow rules of granular materials can be approximated as that of a power-law fluid as given by:

$$\eta^* = KI^{\alpha-1}, \quad (26)$$

where, $K = \mu \sqrt{p^*} I^{-\alpha}$ is the flow consistency and α is the flow behavior index. The flow rules of granular materials are pretty straightforward at high pressures with $\alpha \approx 0$. However, deviations are observed from the power-law behavior at small pressures. More details on the flow rules at large and small pressure are explained in sections 7.1.2 and 7.1.3 respectively.

Figure 10 shows the local apparent viscosity η^* as a function of the inertial number I for different global Bond numbers. The data shown correspond to all the data close to the shear band center for different heights. The inertial number is lowest at an intermediate height, and increases towards surface and base. With increasing inertial number, the apparent shear viscosity decreases, indicating that granular materials flow like non-Newtonian fluids, specifically shear-thinning fluids. It is also evident from the figure that the flow behavior is different at large and small confining pressure.

7.1. Prediction of local apparent viscosity

7.1.1. Prediction of strain rate

Various numerical and experimental results suggest the presence of shear bands in granular materials subjected to relative motion [9, 12]. Often this shear band is considered as a thin layer of localized strain rate, separating rigid blocks of constant velocity. Investigations on the shear band formation reveal that its characteristics are influenced by a number of factors including density, confining pressure, particle size and shape, friction, anisotropy of the material and cohesion [12, 39]. The shear band thickness and the distance from the center decrease as the confining pressure increases [2]. Constitutive relations exist for many shear band properties [32], which suggests a pathway to finding analytical solutions.

In this section, we discuss an analytical approach to get stress and strain rate correlations from the physics of granular materials and compare our analytical solution with the numerical results for different wet cohesion using the generalized μ function for the macroscopic friction, see equations (22) and (25). The magnitude of the strain rate is given by equation (4). It is assumed that the velocity component u_ϕ is slowly varying in z -direction ($\partial u_\phi / \partial z \approx 13\%$ of $(\partial u_\phi / \partial r - u_\phi / r)$ in the shear band center), so $\partial u_\phi / \partial z$ is small (by one order of magnitude) and is neglected with an approximation, so that

$$\dot{\gamma} \approx \frac{1}{2} \left(\frac{\partial u_\phi}{\partial r} - \frac{u_\phi}{r} \right). \quad (27)$$

In the shear band region, the non-dimensionalized angular velocity profile $\omega = u_\phi / (2\pi r \Omega)$ at every height can be well approximated by an error function [4, 5, 8, 23]:

$$\omega = A + B \operatorname{erf} \left(\frac{r - R_c}{W} \right), \quad (28)$$

where $A \approx B \approx 0.5$, W and R_c are the width and the position of the shear band, respectively at different heights. Most surprising is the fact that the fit works equally well for a wide range of I , p^* , Bo etc [39]. Equation (28) substituted in equation (27) can be simplified as a first order expansion of the derivative of the error function as:

$$\dot{\gamma} = \frac{\sqrt{\pi} r \Omega}{W} \exp \left[- \left[\frac{r - R_c}{W} \right]^2 \right]. \quad (29)$$

The shear rate at the center of the shear band ($r = R_c$) is thus given as:

$$\dot{\gamma}_{\max} = \frac{\sqrt{\pi} R_c \Omega}{W}. \quad (30)$$

The pressure for the given geometry is increasing linearly from the free surface, i.e. varies hydrostatically with the depth inside the material. Further, we obtain the non-dimensional inertial number from the predicted strain rate and pressure, so that

$$I_{\max} = \frac{\dot{\gamma}_{\max} d_p}{\sqrt{p/\rho}} \propto \frac{\dot{\gamma}_{\max} d_p}{\sqrt{H - z}}, \quad (31)$$

ignoring the small variations in the bulk density.

7.1.2. Prediction of apparent viscosity of materials under large pressure

The predicted local apparent viscosity from equations (24) and (25) can be simplified with $f_g(p_g^*) \approx 1$ under large pressure, $\mu_t(I) \approx \mu_o$ for quasistatic states and $f_p(p^*) \approx 1$ for the relatively stiff particles ($0.002 < p^* < 0.01$) studied in our system and thus can be written as:

$$\eta^* = \frac{\mu_o \sqrt{p^*}}{I} [1 + aBo]. \quad (32)$$

For dry non-cohesive materials, $Bo = 0$ and $\sqrt{p^*}$ is slowly changing at high pressure. For wet cohesive materials, the magnitude of apparent viscosity is thus determined by the term $f_c(Bo)$. However, the flow behavior index for wet materials is also constant under high confining pressure for the same reason as stated for dry materials as $Bo \propto 1/p$. Table 2 shows the value of the index $\alpha - 1$ for different Bo_g . Under high confining pressure, α is independent of cohesion and $\alpha \approx 0$, $\alpha - 1$ corresponding to the slope of the red dashed-dotted lines in figure 10. Thus, $\eta^* \propto I^{-1}$ and $\alpha \approx 0$ confirms that both dry and wet granular materials behave like a power law fluid under large confining pressure.

7.1.3. Prediction of apparent viscosity of materials under small pressure

Wet cohesive materials confined to small pressure near the surface show more interesting behavior. Here, the pressure and strain rate are very small, i.e. large t_p and t_γ make confining pressure and strain rate less dominant,

Table 2. Table showing the flow behavior index under large pressure constraint (red dashed–dotted lines fitted to figure 10).

Bo_g	0.0	0.06	0.12	0.24	0.36	0.60	1.28	1.94	2.54	3.46
$\alpha - 1$	-0.94	-0.81	-0.92	-0.82	-0.89	-1.00	-0.93	-1.10	-1.23	-1.09

so that t_g and t_c are the two interacting time scales. The rheology is now strongly dependent on the corrections $f_g(p_g^*)$ and $f_c(Bo)$ but not on the correction $f_p(p^*) \approx 1$ ($p^* < 0.005$) under small confining pressure. The strain rate close to the center of the shear band and free surface is almost constant since the shear band is wide so that $f_q \approx 1$ while $\mu_f \approx \mu_o$. We use this simplified constant strain rate to predict the apparent viscosity near the surface of the shear cell where the pressure is very small. The apparent shear viscosity for wet cohesive materials confined to small pressure is more intricate and is predicted by from equations (24) and (25) with $f_p(p^*) \approx 1$ as:

$$\eta^* = \frac{\mu_o \sqrt{p^*}}{I} [1 + aBo] \left[1 - a' \exp\left(-\frac{p_g^*}{p_{go}^*}\right) \right]. \quad (33)$$

Figure 10 shows the prediction of apparent viscosity at small pressure as given by the green solid lines. Non-cohesive materials upto weakly cohesive materials ($Bo_g < 0.60$), at low pressure, are less viscous than those at high pressure, as shown in the figure. For global Bond number $Bo_g = 0.60$, materials for a given inertial number have the same apparent viscosity independent of pressure. For even higher cohesion ($Bo_g > 0.60$), the flow behavior changes qualitatively. Though, the apparent viscosity decreases with the inertial number ($\eta^* \propto I^{-\delta}$), even for cohesive materials, the qualitative decay power δ decreases towards zero ($\delta \rightarrow 0$). For a given inertial number, the material near the surface has higher apparent viscosity than in the bulk and at the base. Materials confined by small pressure thus display reduced shear thinning with increase in cohesion. This is represented by the direction of black arrows marked with Bo_g in figure 10. Thus, granular materials have different shear-thinning properties depending on local confining pressure and Bond number.

7.1.4. Analytical prediction of apparent viscosity

We extract the position and the width of the shear band R_c and W respectively from the fit function in equation (28). Both position and width of the shear band depend on the height in the system and the position moves inwards with increasing height (decreasing pressure). Predictions of the position of the shear band center as a function of height is given in [44]. Since the analytical prediction discussed here is not significantly affected by this varying position of the shear band, we use the mean shear band position \bar{R}_c for our prediction. The shear band moves inward with increase in global Bond number [39]. Thus the mean shear band position \bar{R}_c decreases with increasing Bo_g (not shown here).

The width of the shear band is predicted as function of height as given by [32]:

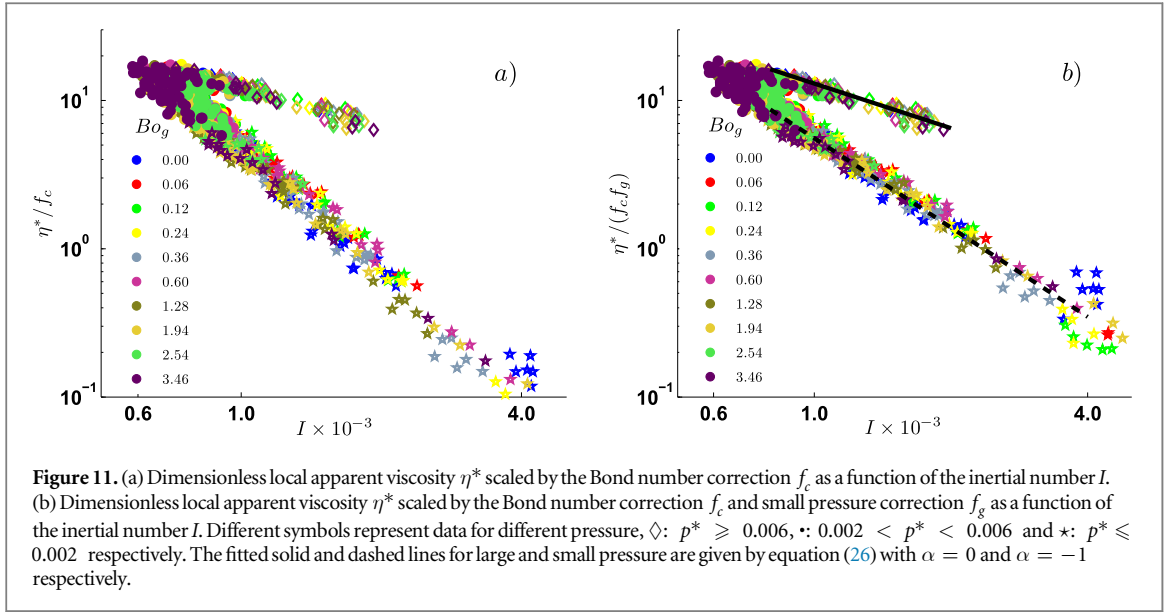
$$W(z) = W_{\text{top}} \left[1 - \left(1 - \frac{z}{H} \right)^2 \right]^\beta, \quad (34)$$

where $\beta = 0.6$ for non-cohesive materials and $0.5 < \beta < 0.7$ for cohesive materials are fitted well by our data. Assuming the pressure varying hydrostatically and the bulk density as $\rho_b \approx 0.6\rho$, we translate equation (34) to W as a function of p . Substituting equations (31) and (34) in (13) and rearranging, we get the inertial number I_{max} in the shear band center as a function of the local pressure p . Further, by substituting p , we get η_{max}^* in the shear band center and thus obtain a quantitatively accurate prediction of η_{max}^* (I_{max}), plotted as blue solid lines and cyan dashed lines in figure 10.

The results show that the analytical solution is in good agreement with our numerical results. Focusing on the slope of the small pressure line, we observe that it changes with increasing cohesion in the same way as shown by numerical data. It is observed from the analytical solution that this change in slope is governed by μ . Thus, the shear-thinning rate for materials under small pressure depends on local friction coefficient, which depends on the corrections $f_g(p_g^*)$ and $f_c(Bo)$.

7.2. Eliminating the effect of cohesion and gravity

Under larger confining pressure (as stated in section 7.1.2), with increase in cohesion, the apparent viscosity of the granular fluid increases, however, the flow behavior remains qualitatively the same even for very high cohesion. For materials confined to large pressure, where \sqrt{p} is slowly varying, the apparent viscosity is inversely proportional to the strain rate and approximately also to the inertial number. At smaller pressure, the materials are more free only under the effect of gravity, with less dominant forces due to particle contacts. Therefore, cohesion is relatively more dominant for higher local Bond numbers, resulting in the qualitative change in shear thinning rate (α). Thus the flow of materials is affected by both dimensionless numbers Bo and



p_g^* at the same time. Then, the granular fluid appears to no longer behave like a power-law fluid. Several of these rheological correction factors make the flow behavior even more nonlinear under small pressure. In order to see the rheology of the granular fluid under small pressure, which is devoid of the effect of these dimensionless numbers, we rescale the local dimensionless apparent viscosity η^* by $f_c(Bo)$ and $f_g(p_g^*)$ and analyze it as a function of inertial number. Figure 11(a) shows the dimensionless apparent viscosity η^* scaled by $f_c(Bo)$ as a function of inertial number for different cohesion. All the data for different cohesion collapse to a single plot for the triad of different pressure scales. Further, we rescale $\eta^*/f_c(Bo)$ by $f_g(p_g^*)$ and plot it as a function of inertial number for different cohesion as shown in figure 11(b). The fitted solid line corresponding to the data at large pressure is given by equation (26) with $\alpha = 0$ and $K \approx 0.01$. Furthermore, the fitted dashed line corresponding to the data at small pressure is given by equation (26) with $\alpha = -1$ and $K \approx 5.6 \times 10^{-6}$. This is explained theoretically by substituting p^* in equation (13) and using equation (33) with constant friction coefficient μ_0 yielding:

$$\frac{\eta^*}{f_c(Bo)f_g(p_g^*)} = \frac{\mu_0 \hat{\gamma} d_p^{3/2}}{I^2} \sqrt{\frac{\rho}{k}}. \quad (35)$$

Thus, for slowly varying strain rate at small pressure, η^* is proportional to I^{-2} and is represented by equation (26) with $\alpha = -1$. This eventually explains the earlier observations in [25].

Thus, the flow behavior for granular materials in a simple hypothetical case with high confining stress constant friction coefficient can be approximated by that of a power-law fluid flow behavior. However, for more realistic systems, e.g., unit operations at low stress, several other factors influence the flow rheology, e.g., near to the free surface. Thus, under small pressure, granular materials behave more interestingly and complex than a power-law fluid.

8. Discussions and conclusions

The rheology of dry as well as wet granular materials (in the pendular regime) has been studied by simulations using the discrete element method in steady state shear. Our results show that the conventional $\mu(I)$ rheology must be modified to take into account other factors such as cohesion, contact softness, corrections at small pressures where gravity dominates, and a generalized inertial number dependence for very slow quasi-static flow (creep) in the tails of the shear bands. The trends are combined and shown to collectively contribute to the rheology as multiplicative functions, i.e. ignoring one contribution can lead to inconsistent results. This new generalized rheological model applies to a wide range of parameters from dry non-cohesive to strongly cohesive materials, and contains also both the small and the large pressure limits. Note that additional contributions from viscous forces should be included in case of rapid flow. Our ongoing work shows that the generalized rheology is independent of system configuration, pressure or volume control, in the critical state and is applicable for both homogeneous simple shear and inhomogeneous systems like the split-bottom shear cell. Given this is justified, the shear thinning behavior for granular materials is valid for every locally reached critical state, irrespective of the system configuration for moderate to low pressure and in the dense regime.

Furthermore, we study the apparent viscosity as a function of inertial number for granular fluids of varying cohesive strength. Most strikingly, the cohesive strength not only increases the magnitude of the apparent viscosity, but also decreases the shear thinning rate, but only for material under small confining pressure e.g. close to the free surface. This variable shear thinning behavior of granular materials, close to a free surface, is attributed to the higher local Bond number i.e. it is a low pressure effect. Thus, the flow rheology (friction and apparent viscosity) is predicted by the proposed rheology model for dry and wet granular materials under both low and high confining stress. Further, we develop an analytical solution for the apparent viscosity using the proposed rheology (with some simplifications) and show that the results are in good agreement with our numerical analysis. Materials have less shear thinning with an increase in cohesion as quantified by the high Bond numbers under small confining pressure.

Finally, it is shown that the effect of each of the dimensionless numbers can be eliminated by rescaling, and thus the scaled apparent viscosity of a simple system with a (small) constant friction coefficient is predicted as that of a power-law fluid with Bagnold type scaling with I .

As an outlook, we aim to implement the generalized rheological model in a continuum description of the split-bottom shear cell geometry. A successful implementation is only the first step for validation and paves the way to use this rheological model in industrial applications for material flow descriptions. We aim to also include higher order effects of the Bond number in the generalized rheology. We included the small pressure (free surface) correction in the rheology, as an effect of gravity. It is to be noted that even in a micro-gravity system, both pressure and gravity change identically and thus the corresponding correction term remains the same as in a system with high gravity. Thus this correction corresponds to an effect active at interfaces or at the free-surface. Next step is to perform the micro-structural analysis [39] also for our system and in particular close to the free surface in order to understand the change of the shear thinning rate. Another open question concerns the creep correction and its relation to the micro-structure and granular temperature. Last, the present rheology has to be merged to kinetic theory in the rapid, collisional flow regime [45], which presents another open challenge.

Acknowledgments

We would like to thank A Singh as we could validate our simulations with his existing rheological dry data. We would also like to thank D Berzi and D Vescovi for their useful suggestions on our rheological models. This work is financially supported by STW Project 12272 ‘Hydrodynamic theory of wet particle systems: Modeling, simulation and validation based on microscopic and macroscopic description’.

Appendix. Summary of the generalized rheological model

Table A1. List of rheological correction functions for application in a continuum model, see equation (22).

Dimensionless numbers	Corrections	Coefficients from fits	Coefficients in [27]
Inertial number (I)	$\mu_I = \mu_o + \frac{\mu_\infty - \mu_o}{1 + I_o/I}$	$\mu_o = 0.16$, $\mu_\infty = 0.40 \pm 0.01$, $I_o = 0.07 \pm 0.007$	$\mu_o = 0.15$, $\mu_\infty = 0.42$, $I_o = 0.06$
Softness (p^*)	$f_p = 1 - (p^*/p_o^*)^\beta$	Taken from [27]	$\beta = 0.50$, $p_o^* = 0.90$
Small pressure (p_g^*)	$f_g = 1 - a' \exp(-p_g^*/p_{go}^*)$	$a' = 0.71 \pm 0.03$, $p_{go}^* = 1.19 \pm 0.05$	
Small inertial number (I)	$f_q = 1 - \exp\left(-\left(\frac{I}{I^*}\right)^{\alpha_1}\right)$	$\alpha_1 = 0.48 \pm 0.07$, $I^* = (4.85 \pm 1.08) \times 10^{-5}$	See [24] for a similar correction
Bond number (Bo)	$f_c = 1 + aBo$	$a = 1.47 \pm 0.17$	

References

- [1] Berger N, Azéma E, Douce J F and Radjai F 2016 Scaling behaviour of cohesive granular flows *Europhys. Lett.* **112** 64004
- [2] Bolton M 1986 The strength and dilatancy of sands *Geotechnique* **37** 219–26
- [3] Bonnoit C, Lanuza J, Lindner A and Clement E 2010 Mesoscopic length scale controls the rheology of dense suspensions *Phys. Rev. Lett.* **105** 108302
- [4] Cohen-Addad S, Höhler R and Pitois O 2013 Flow in foams and flowing foams *Annu. Rev. Fluid Mech.* **45** 241
- [5] Dijkstra J A and van Hecke M 2010 Granular flows in split-bottom geometries *Soft Matter* **6** 2901–7
- [6] Fall A, Bertrand F, Hautemayou D, Mezière C, Moucheron P, Lemaître A and Ovarlez G 2015 Macroscopic discontinuous shear thickening versus local shear jamming in cornstarch *Phys. Rev. Lett.* **114** 098301
- [7] Fall A, Bertrand F, Ovarlez G and Bonn D 2012 Shear thickening of cornstarch suspensions *J. Rheol.* **56** 575–91
- [8] Fenistein D, van de Meent J W and van Hecke M 2004 Universal and wide shear zones in granular bulk flow *Phys. Rev. Lett.* **92** 94301

- [9] Fenistein D and van Hecke M 2003 Kinematics—wide shear zones in granular bulk flow *Nature* **425** 256
- [10] Forterre Y and Pouliquen O 2008 Flows of dense granular media *Annu. Rev. Fluid Mech.* **40** 1–24
- [11] Gu Y, Chialvo S and Sundaresan S 2014 Rheology of cohesive granular materials across multiple dense-flow regimes *Phys. Rev. E* **90** 032206
- [12] Henann D L and Kamrin K 2013 A predictive, size-dependent continuum model for dense granular flows *Proc. Natl Acad. Sci.* **110** 6730–5
- [13] Huang N and Bonn D 2007 Viscosity of a dense suspension in couette flow *J. Fluid Mech.* **590** 497–507
- [14] Huang N, Ovarlez G, Bertrand F, Rodts S, Coussot P and Bonn D 2005 Flow of wet granular materials *Phys. Rev. Lett.* **94** 28301
- [15] Imole O I, Krijgsman D, Weinhart T, Magnanimo V, Montes E C, Ramaioli M and Luding S 2016 Experiments and discrete element simulation of the dosing of cohesive powders in a simplified geometry *Powder Technol.* **287** 108–20
- [16] Jop P, Forterre Y and Pouliquen O 2006 A constitutive law for dense granular flows *Nature* **441** 727–30
- [17] Kamrin K and Koval G 2012 Nonlocal constitutive relation for steady granular flow *Phys. Rev. Lett.* **108** 178301
- [18] Khamseh S, Roux J N and Chevoir F 2015 Flow of wet granular materials: a numerical study *Phys. Rev. E* **92** 022201
- [19] Koval G, Roux J N, Corfdir A and Chevoir F 2009 Annular shear of cohesionless granular materials: from the inertial to quasistatic regime *Phys. Rev. E* **79** 21306
- [20] Kumar N and Luding S 2016 Memory of jamming—multiscale models for soft and granular matter *Granular Matter* **18** 1–21
- [21] Lemaitre A, Roux J N and Chevoir F 2009 What do dry granular flows tell us about dense non-brownian suspension rheology? *Rheol. Acta* **48** 925–42
- [22] Lin N Y C, Guy B M, Hermes M, Ness C, Sun J, Poon W C K and Cohen I 2015 Hydrodynamic and contact contributions to continuous shear thickening in colloidal suspensions *Phys. Rev. Lett.* **115** 228304
- [23] Luding S 2008 Cohesive, frictional powders: contact models for tension *Granular Matter* **10** 235–46
- [24] Luding S 2008 Constitutive relations for the shear band evolution in granular matter under large strain *Particuology* **6** 501–5
- [25] Luding S 2008 The effect of friction on wide shear bands *Particulate Sci. Technol.* **26** 33–42
- [26] Luding S and Alonso-Marroquin F 2011 The critical-state yield stress (termination locus) of adhesive powders from a single numerical experiment *Granular Matter* **13** 109–19
- [27] Luding S, Singh A, Roy S, Vescovi D, Weinhart T and Magnanimo V 2017 From particles in steady state shear bands via micro-macro to macroscopic rheology laws *Proceedings of the 7th International Conference on Discrete Element Methods (Springer Proceedings in Physics 188)* ed X Li, Y Feng and G Mustoe (Singapore: Springer) pp 13–9
- [28] Mani R, Kadau D, Or D and Herrmann H J 2012 Fluid depletion in shear bands *Phys. Rev. Lett.* **109** 248001
- [29] Mari R, Seto R, Morris J F and Denn M M 2015 Discontinuous shear thickening in brownian suspensions by dynamic simulation *Proc. Natl Acad. Sci.* **112** 15326–30
- [30] MiDi G D R 2004 On dense granular flows *Eur. Phys. J. E* **14** 341–65
- [31] Pouliquen O, Cassar C, Jop P, Forterre Y and Nicolas M 2006 Flow of dense granular material: towards simple constitutive laws *J. Stat. Mech.* P07020
- [32] Ries A, Wolf D E and Unger T 2007 Shear zones in granular media: three-dimensional contact dynamics simulations *Phys. Rev. E* **76** 051301
- [33] Roy S, Luding S and Weinhart T 2015 Towards hydrodynamic simulations of wet particle systems *Proc. Eng.* **102** 1531–8
- [34] Roy S, Luding S and Weinhart T 2017 Effect of cohesion on local compaction and granulation of sheared granular materials *Eur. Phys. J. Web Conf.* (submitted)
- [35] Roy S, Singh A, Luding S and Weinhart T 2015 Micro-macro transition and simplified contact models for wet granular materials *Comput. Part. Mech.* **3** 449–62
- [36] Scheel M, Seemann R, Brinkmann M, Di Michiel M, Sheppard A and Herminghaus S 2008 Liquid distribution and cohesion in wet granular assemblies beyond the capillary bridge regime *J. Phys.: Condens. Matter* **20** 494236
- [37] Schöllmann S 1999 Simulation of a two-dimensional shear cell *Phys. Rev. E* **59** 889–99
- [38] Schwarze R, Gladkyy A, Uhlig F and Luding S 2013 Rheology of weakly wetted granular materials: a comparison of experimental and numerical data *Granular Matter* **15** 455–65
- [39] Singh A, Magnanimo V, Saitoh K and Luding S 2014 Effect of cohesion on shear banding in quasistatic granular materials *Phys. Rev. E* **90** 022202
- [40] Singh A, Magnanimo V, Saitoh K and Luding S 2015 The role of gravity or pressure and contact stiffness in granular rheology *New J. Phys.* **17** 043028
- [41] Thornton A, Weinhart T, Luding S and Bokhove O 2012 Frictional dependence of shallow-granular flows from discrete particle simulations *Eur. Phys. J. E* **35** 1–8
- [42] Thornton A, Weinhart T, Luding S and Bokhove O 2012 Modeling of particle size segregation: calibration using the discrete particle method *Int. J. Mod. Phys. C* **23** 124001
- [43] Thornton A, Weinhart T, Ogarko V and Luding S 2013 Multi-scale modeling of multi-component granular materials *Comput. Methods Mater. Sci.* **13** 1–16
- [44] Unger T, Török J, Kertész J and Wolf D E 2004 Shear band formation in granular media as a variational problem *Phys. Rev. Lett.* **92** 214301
- [45] Vescovi D and Luding S 2016 Merging fluid and solid granular behavior *Soft Matter* **12** 8616–28
- [46] Wagner N J and Brady J F 2009 Shear thickening in colloidal dispersions *Phys. Today* **62** 27–32
- [47] Wang X, Zhu H P and Yu A B 2012 Microdynamic analysis of solid flow in a shear cell *Granular Matter* **14** 411–21
- [48] Clift R, Grace J R and Weber M E 1978 *Bubbles, Drops, and Particles* (New York: Academic) pp 171–202
- [49] Weinhart T, Hartkamp R, Thornton A and Luding S 2013 Coarse-grained local and objective continuum description of three-dimensional granular flows down an inclined surface *Phys. Fluids* **25** 070605
- [50] Weinhart T, Thornton A, Luding S and Bokhove O 2012 From discrete particles to continuum fields near a boundary *Granular Matter* **14** 289–94
- [51] Willett C D, Adams M J, Johnson S A and Seville J 2000 Capillary bridges between two spherical bodies *Langmuir* **16** 9396–405
- [52] Woldhuis E, Tighe B P and Saarloos W 2009 Wide shear zones and the spot model: Implications from the split-bottom geometry *Eur. Phys. J. E* **28** 73–8